Multi-Objective Reinforcement Learning for Efficient Tactical Decision Making for Trucks in Highway Traffic

Deepthi Pathare[1,3] , **Leo Laine**[2,3] , **Morteza Haghir Chehreghani**[1]

[1]Department of Computer Science and Engineering, Chalmers University of Technology and University of Gothenburg, Sweden

[2]Department of Mechanics and Maritime Sciences, Chalmers University of Technology, Sweden

[3]Safe and Efficient Driving, Volvo Group of Trucks Technology, Sweden

pathare@chalmers.se

Abstract

Balancing safety, efficiency, and operational costs in highway driving poses a challenging decision-making problem for heavy-duty vehicles. A central difficulty is that conventional scalar reward formulations, obtained by aggregating these competing objectives, often obscure the structure of their trade-offs. We present a Proximal Policy Optimization based multi-objective reinforcement learning framework that learns a continuous set of policies explicitly representing these trade-offs and evaluates it on a scalable simulation platform for tactical decision making in trucks. The proposed approach learns a continuous set of Pareto-optimal policies that capture the trade-offs among three conflicting objectives: safety, quantified in terms of collisions and successful completion; energy efficiency and time efficiency, quantified using energy cost and driver cost, respectively. The resulting Pareto frontier is smooth and interpretable, enabling flexibility in choosing driving behavior along different conflicting objectives. This framework allows seamless transitions between different driving policies without retraining, yielding a robust and adaptive decision-making strategy for autonomous trucking applications.

1 Introduction

Autonomous driving requires real-time decision-making under uncertainty, where multiple conflicting objectives must be simultaneously balanced [Campbell *et al.*, 2010; Abdallaoui *et al.*, 2023]. For heavy-duty trucks, this challenge becomes even more pronounced due to their large size, high fuel consumption, long braking distances, and the severe consequences that can result from even minor control errors [Zhang *et al.*, 2020; Engström *et al.*, 2018]. Designing control architectures that can adaptively manage these trade-offs, prioritizing safety in dense traffic and fuel economy on open highways, and benchmarking them in controlled simulations are therefore essential for the reliable and economically viable deployment of autonomous trucks [Schwarting *et al.*, 2018; Eleonora *et al.*, 2023].

Traditional approaches to modeling autonomous driving have relied on rule-based architectures, optimization-based control, and data-driven learning methods. Early rule-based systems relied on hand-crafted decision rules and safety constraints to govern vehicle behavior and ensure compliance with traffic rules, offering strong interpretability and real-time performance but limited adaptability to complex or rapidly changing traffic scenarios [Paden *et al.*, 2016]. More recent work has explored the use of interpretable decision-tree models for specific sub-tasks such as goal recognition and trajectory prediction, enabling fast inference and formal verification of prediction behavior [Brewitt *et al.*, 2021]. Optimization-based frameworks, most notably Model Predictive Control (MPC) [Isaksson Palmqvist, 2016], have also been applied to autonomous vehicle maneuvers [Nilsson *et al.*, 2015; Musa *et al.*, 2021]. While these methods perform well in motion-planning tasks, they often require accurate models of the environment and struggle to scale with the increasing complexity of real-world traffic.

A number of these challenges have been mitigated through Reinforcement Learning (RL), which has emerged as a promising alternative capable of learning control policies directly from interactions with traffic environments. Deep RL agents have demonstrated strong performance in tasks such as lane changing, merging, and adaptive cruise control, discovering policies that can outperform hand-crafted control strategies in complex and dynamic highway environments [Kiran *et al.*, 2022; Hoel *et al.*, 2020; Pathare *et al.*, 2023]. However, most RL approaches in autonomous driving rely on a single scalar reward function that combines multiple objectives such as safety, comfort, and energy efficiency. Although this simplification facilitates training, it constrains the learned policy to a fixed trade-off between objectives.

A recent study [Pathare *et al.*, 2026] has investigated this paradigm in detail for heavy duty vehicles. It showed that deep reinforcement learning can be applied effectively to tactical decision making for autonomous trucks for lane changing and adaptive cruise control in highway traffic simulations. The authors propose a hierarchical control architecture where RL handles high-level tactical decisions using reward functions incorporating safety, efficiency, and total operational cost, while low-level control is managed by physics-based models. While this study established the practical feasibility of RL for tactical driving, it also reveals a key limitation:

achieving optimal performance using a single scalar reward is challenging. Agents learn stable behaviors with simpler, safety-focused rewards but struggle when the reward must jointly capture safety, efficiency, and operational costs. Similar challenges have also been reported in other studies, where competing objectives are difficult to balance within a single reward signal and lead to poor generalization [Abouelazm *et al.*, 2024; Knox *et al.*, 2023].

Multi-Objective Reinforcement Learning (MORL) can potentially address this problem by explicitly optimizing multiple objectives without collapsing them into a single scalar. See Appendix A for a review of various MORL methods including evolutionary optimization and preference-conditioned methods.

In the broader autonomous driving literature, MORL has been applied to explicitly balance competing objectives. For example, the paper [He and Lv, 2023] proposed an Actor-Critic MORL for user-preference-conditioned decision-making that trades off the energy consumption and travel efficiency. MORL for highway decision making has been proposed in [Xu *et al.*, 2018], and Ref. [Surmann *et al.*, 2025] demonstrate adaptive MORL policies that adjust to user preferences. Although these studies demonstrate the potential of MORL for balancing multiple objectives, they focus primarily on passenger vehicles and overlook the specific operational challenges of heavy-duty trucks. These challenges become especially significant when realistic reward functions, such as Total Cost of Operation (TCOP), are considered.

In this paper, we address this gap by developing a multi-objective reinforcement learning framework specifically tailored for heavy-duty vehicles. Our approach builds on the Generalized Policy Improvement with Linear Support (GPI-LS) framework introduced by Alegre *et al.* [Alegre *et al.*, 2023], which formulates preference prioritization as a principled optimization problem with theoretical guarantees and achieves faster convergence and higher utility across multiple objectives than prior MORL methods. We extend this GPI-based prioritization, originally implemented in a value-based RL setting, to a policy-gradient approach and apply it to the multi-objective tactical decision-making problem for trucks. Proximal Policy Optimization (PPO) is used as the underlying RL algorithm due to its proven performance in tactical driving tasks [Pathare *et al.*, 2023] and many other domains such as fine-tuning Large Language Models. To handle multiple objectives, we develop a multi-objective PPO (MOPPO) architecture with a vector-valued critic and per-objective action logits, applying scalarization only at the loss level. This design preserves the individual structure of each objective during learning, facilitates efficient policy improvement across different preference configurations, and allows the reuse of experiences collected under varying trade-off settings, making learning both stable and sample-efficient.

We validate the proposed framework on a realistic highway driving task involving adaptive cruise control and lane change decision making for an autonomous truck. The problem is formulated with three inherently conflicting objectives, namely, safety, time efficiency and energy efficiency, reflecting operational priorities in commercial trucking. Using a high-fidelity microscopic traffic simulator, we demonstrate that the proposed method efficiently approximates the convex coverage set of the Pareto frontier and enables dynamic, preference-aware policy selection. The proposed MORL framework and the custom RL environment for autonomous truck driving are released as open source, enabling reproducibility and facilitating future research in multi-objective decision making and autonomous truck driving.

2 Problem Formulation

2.1 Decision Making in Traffic Environment

We study the problem of tactical decision making for a heavy-duty truck in a stochastic highway environment, with multiple conflicting objectives. Tactical decisions include adaptive cruise control and lane changes, and with the objectives to balance safety, time efficiency, and energy efficiency.

The environment is implemented using the open-source traffic simulator SUMO (Simulation of Urban MObility), which provides realistic microscopic vehicle dynamics. The simulation consists of a three-lane highway segment populated by mixed traffic, including passenger cars and trucks. The ego vehicle is modeled as a tractor–semitrailer combination with realistic dynamics. To maintain a stationary traffic distribution around the ego vehicle, a moving window is used, with vehicles dynamically re-spawned at the boundaries. Traffic density is varied across experiments to assess robustness under different congestion levels. Additional details of traffic modeling with parameters and illustrations are provided in Appendix B.

2.2 Multi-Objective Reinforcement Learning

The tactical decision-making problem is inherently multi-objective: strategies that improve travel time often increase energy consumption or safety risk, while conservative driving may degrade operational efficiency. To explicitly capture these trade-offs, we formulate the problem within a multi-objective reinforcement learning (MORL) framework.

The environment is modeled as a Multi-Objective Markov Decision Process (MOMDP), defined by the tuple $\mathcal{M} = (\mathcal{S}, \mathcal{A}, p, \gamma, \mathbf{r})$ where $\mathcal{S}$ and $\mathcal{A}$ denote the state and action spaces, respectively, and $p(\cdot|s, a)$ is the transition probability distribution over next states given the current state–action pair (s, a). The reward function $\mathbf{r} : \mathcal{S} \times \mathcal{A} \times \mathcal{S} \to \mathbb{R}^d$ is vector-valued, with d components corresponding to distinct objectives. The agent's experience thus consists of transitions $(s_t, a_t, s_{t+1}, \mathbf{r}_{t+1})$, where $\mathbf{r}_t = (r_t^{(1)}, \ldots, r_t^{(d)})$ quantifies the instantaneous contributions to each objective. $\gamma \in [0, 1)$ is a discount factor.

A policy $\pi : \mathcal{S} \to \mathcal{A}$ defines the agent's decision rule, mapping states to actions, and value function of the policy is defined as,

$$\mathbf{V}^\pi(s) = \mathbb{E}_\pi \left[\sum_{t=0}^{\infty} \gamma^t \mathbf{r}_{t+1} \mid s_t = s \right]. \tag{1}$$

where the value function $\mathbf{V}^\pi(s) \in \mathbb{R}^d$ is vector valued.

Optimality is defined in terms of Pareto dominance: a policy π' dominates π if it performs at least as well in all objectives and strictly better in at least one. The set of non-

dominated value vectors forms the Pareto frontier, representing all achievable trade-offs beyond which improvement in one objective necessarily degrades another. MORL aims to approximate this frontier rather than identifying a single optimal policy.

User preferences are incorporated via a scalarization function or utility function, $u : \mathbb{R}^d \to \mathbb{R}$, which maps the multi-objective value vector to a scalar utility according to user-defined preferences. We adopt linear scalarization,

$$u(\mathbf{V}^\pi; \mathbf{w}) = \mathbf{w}^\top \mathbf{V}^\pi = \sum_{i=1}^{d} w_i V_i^\pi, \qquad (2)$$

where the weight vector $\mathbf{w}$ lies on the unit simplex. Each weight vector defines a single-objective optimization problem with scalarized rewards $\mathbf{r_w}(s, a, s') = \mathbf{w}^\top \mathbf{r}(s, a, s')$. The set of policies that maximize the scalarized return for some $\mathbf{w}$ forms the Convex Hull (CH), and the minimal subset containing one optimal policy per weight vector is the Convex Coverage Set (CCS), providing a compact approximation of all linearly Pareto-optimal solutions.

This formalism provides a general foundation for multi-objective learning. It allows policies to be optimized according to different user-defined trade-offs, facilitates the quantification of competing objectives, and offers a structured approach to characterize and navigate Pareto-efficient behaviors in complex systems.

2.3 Reinforcement Learning Environment

The overall architecture integrates MORL with model-based low-level controllers, ensuring both strategic adaptability and safety. The MORL agent performs high-level tactical decisions, such as initiating lane changes or adjusting desired speed and time gaps. Low-level controllers execute these commands using established models: the Intelligent Driver Model (IDM) for longitudinal control and the LC2013 model for lateral maneuvers. This hierarchical structure ensures dynamically feasible policies and mitigates uncertainty in safety-critical decisions. Full details of the architecture, action space, and observation space are provided in Appendix C.

The agent optimizes three primary objectives that reflect the essential trade-off in highway driving between safety, time efficiency and energy efficiency:

1. **Safety:** Avoid collisions and successfully reach the target within a finite horizon.

2. **Time Efficiency:** Minimize the driver cost, which is a function of travel time, encouraging the agent to reach the target as quickly as possible.

3. **Energy Efficiency:** Minimize the energy cost, encouraging the agent to adopt energy efficient driving maneuvers.

These objectives jointly define a three-dimensional reward vector given by:

$$\mathbf{r_t} = [I_{tar} R_{tar} - I_c P_c, -C_{dr}\Delta t, -C_{el}e_t]^T \qquad (3)$$

where I is an indicator function, R_{tar} is the reward for reaching the target, P_c is the penalty for collision, C_{dr} is the driver

cost per second, Δt is the duration of a timestep, C_{el} is the energy cost per kwh and e_t is the energy consumed in kwh at time step t. Detailed computations and parameter values are provided in Appendix D.

3 Methodology

3.1 GPI-Based Multi-Objective Reinforcement Learning

The procedure presented in Algorithm 1 iteratively constructs a set of policies $\Pi = \{\pi(a|s, \mathbf{w})\}$ whose associated value vectors $\boldsymbol{V}$ approximate the CCS. At each iteration, the algorithm selects a weight vector $\mathbf{w}$ and learns a policy $\pi_\mathbf{w}$ that optimizes the corresponding scalarized objective. The resulting policy and its value vector are then added to the existing sets, progressively refining the approximation of the CCS. This procedure extends the GPI-LS framework in [Alegre *et al.*, 2023] to a policy-gradient RL setting.

Algorithm 1 GPI Linear Support (GPI-LS) with Multi-Objective PPO

Require: MOMDP M
1: Initialize: Weight support $\mathcal{M} \leftarrow \{\}$, Value vectors $\mathcal{V} \leftarrow \{\}$
2: $(\pi_\mathbf{w}, v^{\pi_\mathbf{w}}) \leftarrow \text{MOPPO}(\mathbf{w} = [1, 0, \ldots, 0]^\top)$
3: $\mathcal{V} \leftarrow \{v^{\pi_\mathbf{w}}\}, \quad \mathcal{M} \leftarrow \{\mathbf{w}\}$
4: **for** $i = 1$ to N **do**
5: $\quad \mathcal{W}_{\text{corner}} \leftarrow \text{CornerWeights}(\mathcal{V}) \setminus \mathcal{M}$
6: $\quad \mathbf{w} \leftarrow \arg\max_{\mathbf{w} \in \mathcal{W}_{\text{corner}}}(\hat{v}_\mathbf{w}^{\text{opt}} - \max_{\pi \in \Pi} v_\mathbf{w}^\pi)$
7: $\quad \mathcal{M}' \leftarrow \text{Unique}\left(\mathcal{M} \cup \text{TopK}(\mathcal{W}_{\text{corner}}) \cup \{\mathbf{w}\}\right)$
8: $\quad (\pi_\mathbf{w}, v^{\pi_\mathbf{w}}, \text{done}) \leftarrow \text{MOPPO}(\mathbf{w}, \mathcal{M}')$
9: $\quad \text{Add } \{\mathbf{w}' \in \mathcal{M}'\} \text{ to } \mathcal{M} \text{ and } \{v^{\pi_{\mathbf{w}'}} \mid \mathbf{w}' \in \mathcal{M}'\} \text{ to } \mathcal{V}$
10: $\quad \mathcal{V}, \mathcal{M} \leftarrow \text{RemoveDominated}(\mathcal{V}, \mathcal{M})$
11: **end for**

Weight selection in each iteration is guided by the concept of *corner weights* [Alegre *et al.*, 2023]. Let $\mathcal{V} = \{\mathbf{v}^{\pi_i}\}_{i=1}^n$ denote the set of multi-objective value vectors corresponding to n trained policies. The corner weights $\mathcal{W}_{\text{corner}} \subset \mathbb{R}^d$ are obtained from the vertices of a polyhedron P defined as:

$$P = \left\{ \mathbf{x} \in \mathbb{R}^{d+1} \,\middle|\, \mathbf{V}^+\mathbf{x} \leq \mathbf{0}, \, \sum_i w_i = 1, \, w_i \geq 0, \, \forall i \right\}, \qquad (4)$$

where $\mathbf{V}^+$ is a matrix whose rows store the elements of $\mathcal{V}$, augmented by a column vector of -1s. Each vector $\mathbf{x} = (w_1, \ldots, w_d, v_\mathbf{w})$ in P corresponds to a candidate weight vector $\mathbf{w}$ and its scalarized value $v_\mathbf{w}$.

Intuitively, corner weights are the weight vectors for which the policy selected in the maximization $\max_{\pi \in \Pi} v_\mathbf{w}^\pi$ changes. These are weight vectors for which two or more policies in Π share the same value with respect to the above-mentioned maximization.

Let $\Pi = \{\pi_i\}_{i=1}^n$ be a set of n policies with corresponding value vectors $\mathcal{V} = \{\mathbf{v}^{\pi_i}\}_{i=1}^n$. Let $\Delta(\mathbf{w}, \Pi) = v_\mathbf{w}^* - \max_{\pi \in \Pi} v_\mathbf{w}^\pi$ be the utility loss of weight vector $\mathbf{w} \in \mathcal{W}$ given the policy set Π; that is, the difference between the value of

the optimal policy for $\mathbf{w}$ and the value that can be obtained if using one of the policies in Π for solving $\mathbf{w}$. Then, a weight vector $\mathbf{w} \in \arg\max_{\mathbf{w} \in \mathcal{W}} \Delta(\mathbf{w}, \Pi)$ is one of the corner weights of $\mathcal{V}$.

We estimate the optimal policy for computing above utility loss using Generalized Policy Improvement (GPI) [Barreto *et al.*, 2017]. For value-based algorithms, GPI policy is defined as:

$$\pi^{\text{GPI}}(s; \mathbf{w}) \in \arg\max_{a \in \mathcal{A}} \max_{\pi \in \Pi} q_{\mathbf{w}}^{\pi}(s, a) \qquad (5)$$

In our PPO-based setting, each policy π outputs action logits rather than Q-values. Therefore, instead of estimating optimal policy based on scalarized action-values, we estimate it based on scalarized action logits derived from the PPO policy networks as given below:

$$\hat{\pi}^{\text{opt}}(s; \mathbf{w}) \in \arg\max_{a \in \mathcal{A}} \max_{\pi \in \Pi} z(a \mid s, \mathbf{w}) \qquad (6)$$

We iteratively select the corner weight $\mathbf{w} \in \mathcal{W}_{\text{corner}}$ that guarantees maximum possible improvement given by:

$$\mathbf{w} \leftarrow \arg\max_{\mathbf{w} \in \mathcal{W}_{\text{corner}}} \left(\hat{v}_{\mathbf{w}}^{\text{opt}} - \max_{\pi \in \Pi} v_{\mathbf{w}}^{\pi} \right) \qquad (7)$$

where $\hat{v}_{\mathbf{w}}^{\text{opt}}$ is the scalarized value of estimated optimal policy. Then, the policy is updated using this $\mathbf{w}$ to maximize the scalarized return.

We choose PPO-based framework to optimize the policy $\pi_{\mathbf{w}}$ at every iteration as described in the following section.

3.2 Multi-Objective Proximal Policy Optimization (MOPPO)

In Algorithm 2, we extend the PPO [Schulman *et al.*, 2017] to handle multi-objective learning by incorporating weight-conditioned actor and critic networks. Our algorithm follows the standard clipped PPO update, but modifies the policy and value function estimation to support multi-dimensional rewards and scalarization using weight vectors. See Figure 1 for a schematic overview of the proposed MOPPO framework. It consists of the following:

1. **Weight-conditioned feature extraction:** The observation features and the user-specified preference vector $\mathbf{w} \in \mathbb{R}^d$ are independently encoded using multi-layer perceptrons (MLPs), and their resulting feature representations are combined element-wise. This conditioning mechanism modulates the state representation according to the preference vector, activating different feature subspaces and allowing the policy network to adapt its behavior to the specified trade-off weights.

2. **Multi-objective actor:** The actor outputs a set of action logits $\mathbf{Z}(a \mid s) \in \mathbb{R}^{|\mathcal{A}| \times d}$, one per reward dimension. These logits are scalarized by $\mathbf{w}$ to obtain a single distribution over actions, from which actions are sampled.

3. **Action Masking:** The policy employs an action-masking mechanism conditioned on the current state to prevent invalid decisions and limit exploration to feasible actions. This approach helps stabilize training and improves sample efficiency. The environment provides

---

Algorithm 2 Multi-Objective PPO Training (Single Iteration)

Require: policy parameters $\boldsymbol{\theta}$, value parameters $\boldsymbol{\phi}$, selected corner weight $\mathbf{w}$, set of top $\mathcal{K}$ corner weights $\mathcal{W}$, steps per iteration N_S

1: **Initialize:** replay buffer $\mathcal{D} \leftarrow \emptyset$, $\mathbf{w}_t \leftarrow \mathbf{w}$
2: **for** each environment step $t = 1, \ldots, N_S$ **do**
3:      Sample action $a_t \sim \pi_\theta(a \mid s_t, \mathbf{w}_t)$ and estimate value $\mathbf{v}_t = V_\phi(s_t, \mathbf{w}_t)$
4:      Execute a_t in the environment to obtain $(\mathbf{r}_t, s_{t+1}, \mathbf{done}_t)$
5:      Store $(s_t, a_t, \log \pi_\theta(a_t \mid s_t, \mathbf{w}_t), \mathbf{r}_t, \mathbf{done}_t, \mathbf{v}_t, \mathbf{w}_t)$ in $\mathcal{D}$
6:      **if** episode terminates **then**
7:          Sample new $\mathbf{w}_t \sim \mathcal{W}$ and reset environment
8:      **end if**
9: **end for**
10: Compute vector advantage estimates $\hat{\mathbf{A}}_t$ using $\text{GAE}(\gamma, \lambda)$
11: Scalarize advantages: $A_t^{(s)} = \mathbf{w}_t^\top \hat{\mathbf{A}}_t = \sum_{i=1}^d w_{t,i} \hat{A}_{t,i}$
12: **for** each update epoch **do**
13:      Sample minibatches from $\mathcal{D}$ and update (θ, ϕ) by minimizing:
$$\mathcal{L}_t^{CLIP+VF+S}(\boldsymbol{\theta}, \boldsymbol{\phi}) = \mathcal{L}_t^{CLIP}(\boldsymbol{\theta}) + c_1 \mathcal{L}_t^{VF}(\boldsymbol{\phi}) - c_2 \mathcal{S}(\pi_{\boldsymbol{\theta}})$$
14: **end for**
15: **Output:** Updated policy $\pi_{\boldsymbol{\theta}}$ and value function $V_{\boldsymbol{\phi}}$

---

a binary mask identifying valid and feasible actions, and logits corresponding to infeasible actions are assigned a large negative value prior to the softmax operation, ensuring their selection probability becomes effectively zero.

4. **Multi-objective critic:** The critic outputs a vector-valued estimate $V(s) \in \mathbb{R}^d$, predicting the expected return for each reward dimension.

5. **Rollout Buffer:** At each iteration, MOPPO trains the network based on the selected corner weight $\mathbf{w}_t$ that gives maximum improvement as mentioned in Section 3.1 along with top $\mathcal{K}$ other corner weights. The algorithm interacts with the environment to gather trajectories conditioned on a weight, either the selected corner weight $\mathbf{w}_t$ or a weight vector sampled uniformly from $\mathcal{W}$, each with probability 0.5. Each transition $(s_t, a_t, \log \pi(a_t|s_t, \mathbf{w}_t), \mathbf{r}_t, \text{done}_t, \mathbf{V}(s_t), \mathbf{w}_t)$ is stored in a rollout buffer. The collected data are then used to compute the objective function and update the networks as described next.

6. **Optimization:** The trainable parameters of the policy and value networks, denoted by $\boldsymbol{\theta}$ and $\boldsymbol{\phi}$, are updated by minimizing the PPO-style objective:
$$\mathcal{L}_t^{CLIP+VF+S}(\boldsymbol{\theta}, \boldsymbol{\phi}) = \mathcal{L}_t^{CLIP}(\boldsymbol{\theta}) + c_1 \mathcal{L}_t^{VF}(\boldsymbol{\phi}) - c_2 \mathcal{S}(\pi_{\boldsymbol{\theta}}) \qquad (8)$$

where $\mathcal{L}_t^{CLIP}(\boldsymbol{\theta})$ is the clipped surrogate objective, $\mathcal{L}_t^{VF}(\boldsymbol{\phi})$ is the squared-error value loss, $\mathcal{S}(\pi_{\boldsymbol{\theta}})$ denotes entropy bonus, and c_1, c_2 are weighting coefficients for
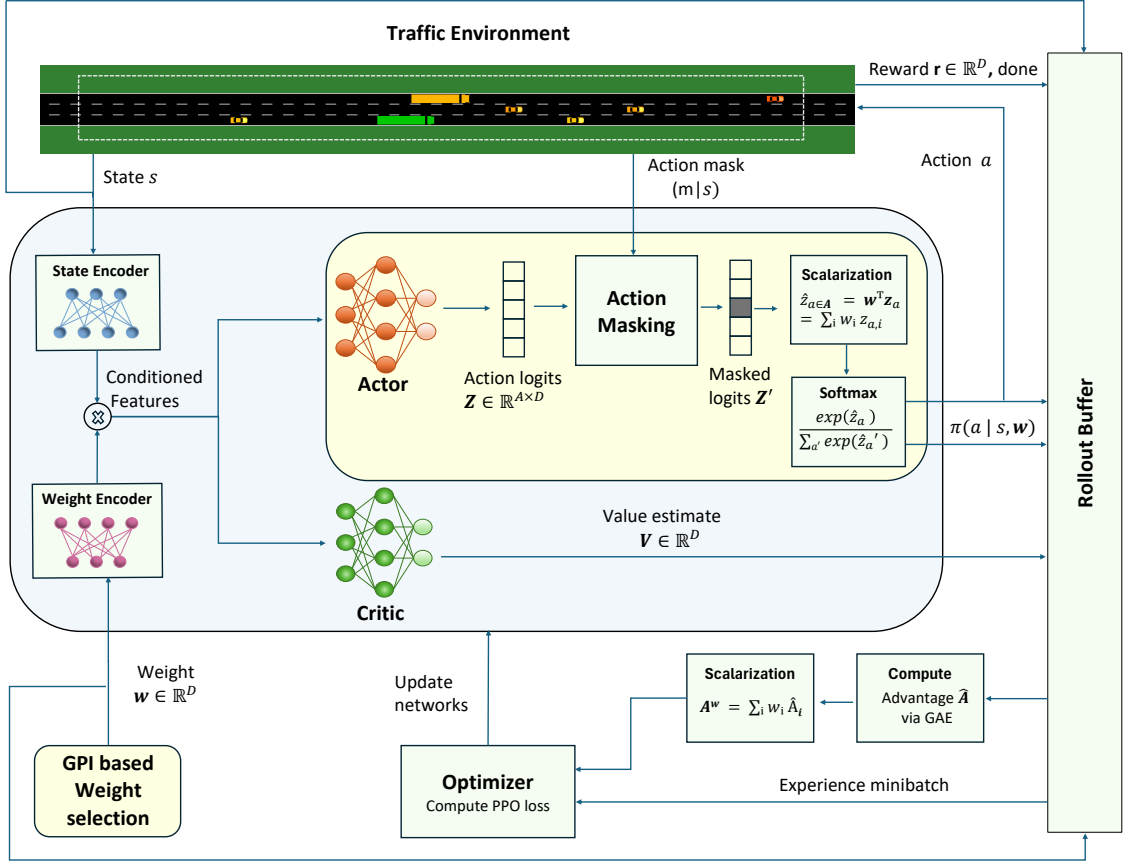
Figure 1: Multi-Objective PPO Framework.

the value loss and entropy bonus, respectively.

$$\mathcal{L}_t^{CLIP}(\boldsymbol{\theta}) = \mathbb{E}\Big[\min\Big(\rho_t(\boldsymbol{\theta})\,A_t^{(s)},$$
$$\text{clip}\big(\rho_t(\boldsymbol{\theta}), 1-\epsilon, 1+\epsilon\big)\,A_t^{(s)}\Big)\Big] \quad (9)$$

where

$$\rho_t(\boldsymbol{\theta}) = \frac{\pi_{\boldsymbol{\theta}}(a_t \mid s_t, \mathbf{w}_t)}{\pi_{\boldsymbol{\theta}_{\text{old}}}(a_t \mid s_t, \mathbf{w}_t)}, \quad A_t^{(s)} = \mathbf{w}_t^\top \hat{\mathbf{A}}_t. \quad (10)$$

The vector $\hat{\mathbf{A}}_t \in \mathbb{R}^d$ denotes the multi-objective advantage computed using Generalized Advantage Estimation (GAE-λ) [Schulman *et al.*, 2015].

3.3 Safety Filter for Lane Changes via Action Masking

To ensure that the ego vehicle performs lane changes only when it is safe to do so, we propose a rule-based safety filter based on time-gap and braking-feasibility constraints. A lane change action from the ego's current lane ℓ_{ego} to a target lane ℓ_{target} is permitted only if sufficient longitudinal gaps exist both ahead of and behind the ego vehicle in target lane. The lane change action is masked out otherwise as described in Section 3. A lane change to left when ego vehicle is on the left-most lane and a lane change to right when vehicle is on the right-most lane are also filtered out.

We evaluate the safety of a candidate lane change using a kinematic, gap-based safety filter that explicitly accounts for finite vehicle dimensions, relative velocities, and the fact that the ego vehicle occupies both the current and target lanes during the maneuver. All longitudinal distances are measured between front bumpers unless stated otherwise.

The lane change duration is given by

$$T_{\text{lc}} = \frac{w_{\text{lane}}}{v_{\text{lat}}},$$

where w_{lane} is the lane width and v_{lat} is the lateral speed of the ego vehicle. Due to the finite vehicle width w_{ego}, the ego vehicle enters the target lane at

$$t_{\text{enter}} = \frac{w_{\text{lane}} - w_{\text{ego}}}{2v_{\text{lat}}},$$

and fully exits the current lane at

$$t_{\text{exit}} = \frac{w_{\text{lane}} + w_{\text{ego}}}{2v_{\text{lat}}}.$$

The minimum required gap to a leading vehicle is

$$s_{\text{min}}(v, \Delta v) = s_0 + \max\left(0, T_{\text{safe}}v + \frac{v\Delta v}{2\sqrt{a_{\text{max}}b_{\text{safe}}}}\right),$$

as defined in Intelligent Driver Model. Here, a minimum standstill gap s_0 and desired time headway T_{safe} are used to

define safety margins. v is the follower speed, Δv is relative speed with the leading vehicle, $a_{\max}$ and b_{safe} denote maximum acceleration and comfortable deceleration respectively.

From the observation of environment, we identify the nearest leading and following vehicles in both the current and target lanes. A lane change is permitted only if all of the following conditions hold:

1. Front gap in current lane: Let $s_{\text{front,cur}}$ be the distance to the leading vehicle in the current lane. The gap must remain safe until the ego fully exits the current lane:

$$s_{\text{front,cur}} - (v_{\text{ego}} - v_{\text{front,cur}})\, t_{\text{exit}} \geq s_{\min}(v_{\text{ego}}, v_{\text{ego}} - v_{\text{front,cur}}).$$

2. Front gap in target lane: Let $s_{\text{front,tar}}$ denote the distance to the leading vehicle in the target lane. The gap must be safe both when the ego enters the target lane and at the end of the maneuver:

$$s_{\text{front,tar}} - (v_{\text{ego}} - v_{\text{front,tar}})\, t_{\text{enter}} \geq s_{\min}(v_{\text{ego}}, v_{\text{ego}} - v_{\text{front,tar}}),$$

and

$$s_{\text{front,tar}} - (v_{\text{ego}} - v_{\text{front,tar}})\, T_{\text{lc}} \geq s_{\min}(v_{\text{ego}}, v_{\text{ego}} - v_{\text{front,tar}}).$$

3. Rear gap in target lane: Let $s_{\text{rear,target}}$ be the distance from the ego to the following vehicle in the target lane. The gap at lane entry must satisfy

$$s_{\text{rear,tar}} + (v_{\text{rear,tar}} - v_{\text{ego}})\, t_{\text{enter}} \geq s_{\min}(v_{\text{rear,tar}}, v_{\text{rear}} - v_{\text{ego}}).$$

4. Rear-vehicle braking feasibility: If the rear vehicle is faster than the ego ($v_{\text{rear,tar}} > v_{\text{ego}}$), we estimate the time-to-collision

$$\text{TTC} = \frac{s_{\text{rear,tar}}}{v_{\text{rear,tar}} - v_{\text{ego}}}.$$

If $\text{TTC} < T_{\text{lc}}$, the required deceleration to avoid collision is approximated as

$$a_{\text{req}} = \frac{v_{\text{rear,tar}} - v_{\text{ego}}}{\max(\text{TTC} - t_{\text{enter}}, \epsilon)},$$

where ϵ is a small constant for numerical stability. The lane change is allowed only if $a_{\text{req}} \leq b_{\text{safe}}$.

The lane change is executed only when all the above constraints are satisfied, introducing a conservative safety filter that enforces feasible merging conditions, thereby reducing the risk of collisions.

4 Experimental Results

In this section, we present results from experiments conducted using the proposed MORL framework in a custom multi-objective RL environment that we developed for truck driving in a highway simulation. Our GPI-LS MOPPO algorithm is implemented on top of the MORL-Baselines toolkit [Felten *et al.*, 2023]. The implementations of MORL and the environment are provided as open-source[1].

We begin by examining the trade-offs learned by the agent under varying traffic densities. Figure 2 shows the Pareto-optimal policies for zero, medium, and high traffic scenarios.

---

[1]Source Code: https://github.com/deepthi-pathare/morl_and_sumo_gym_env/

Each Pareto front is obtained by evaluating the trained agent over 500 equally spaced weight vectors, averaged across 5 episodes. The resulting Pareto-optimal policies illustrate the trade-offs between energy cost and driver cost, as well as their corresponding successful completion rates. For medium traffic density, we use 0.015 vehicles per meter, which corresponds to 7 vehicles (6 cars and 1 truck) based on the chosen moving window size and heterogeneous vehicle ratio reported in Table 1 in Appendix B. For high traffic density, we use 0.03 vehicles per meter, corresponding to 13 vehicles (11 cars and 2 trucks). Across all traffic settings, a clear and interpretable Pareto structure emerges, demonstrating that the learned policies successfully capture the fundamental conflict between energy cost and driver cost. Notably, the failure rate is zero for all policies across all traffic conditions considered, with success defined as reaching the target within the finite episode horizon.

In the zero-traffic scenario, the environment dynamics and initial conditions are deterministic, so reachability is a deterministic property of a policy: for a fixed policy, episodes either always succeed or always fail. The absence of non-dominated policies in the intermediate region of the Pareto front arises from the structure of the cost function and the speed–cost relationship in the obstacle-free setting. In particular, reducing cruising speed from the high-speed regime leads to a rapid increase in driver cost due to longer travel time, while yielding only marginal reductions in energy cost, as energy consumption varies weakly with speed in this range. Consequently, policies that operate at intermediate speeds incur substantially higher driver cost without achieving proportional energy savings and are therefore dominated by faster cruising policies that achieve similar energy cost with lower driver cost. As a result, no Pareto-optimal solutions emerge in the intermediate region of the cost space.

In contrast, when traffic is present, interactions with other vehicles impose state-dependent speed constraints that introduce variability in both travel time and energy usage. Even policies with similar average speeds can experience different patterns of acceleration, deceleration, and lane changes, resulting in a wider range of achievable cost combinations. This breaks the near-deterministic mapping between speed and cost observed in the zero-traffic case and produces multiple non-dominated policies spanning a broader region of the Pareto front. The successful completion rate remains high for a wide range of trade-offs, indicating that the policies can balance driver and energy costs without compromising the feasibility of the task.

Figure 3 compares the average speed and corresponding cost values of Pareto-optimal policies that achieved a 100% successful completion rate against the analytical optimal speed and cost obtained under the constant-speed assumption. A detailed graph of the analytical results that illustrates how the cost values vary as a function of the speed is given in Appendix E. The analysis indicates that the optimal constant speed is 24.04 m/s, yielding a minimum total cost of 3.68 euros for a distance of 3000 meters (0.0012 euros/m). In the zero-traffic scenario, the learned policies approximately match the analytical baseline, as the absence of interactions allows the truck to maintain a speed with mini-
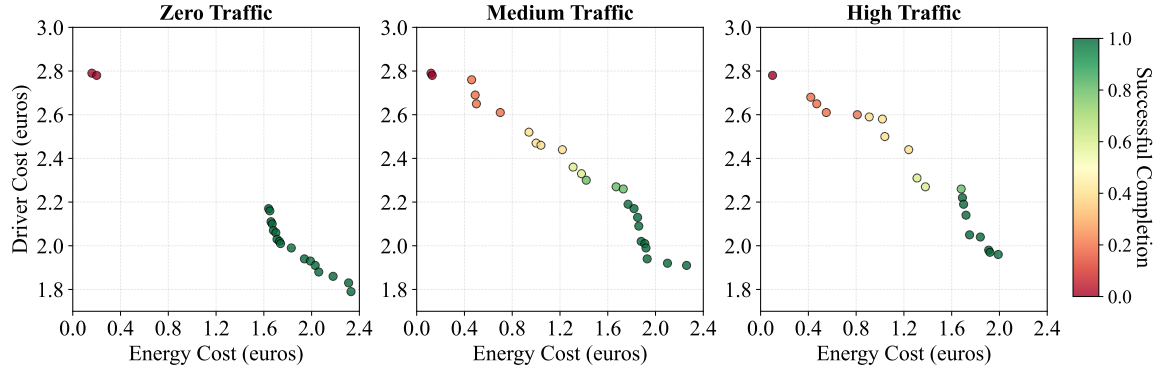
Figure 2: Pareto Front showing the trade off between driver cost and energy cost in three different traffic settings, along with the success rate.
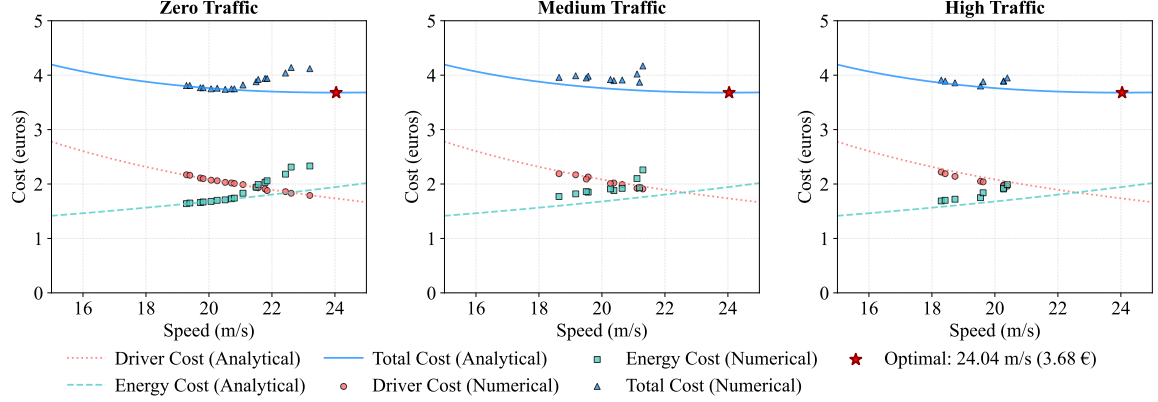

Figure 3: Comparison of average speed and cost values from Pareto-optimal policies with 100% success rate with the analytical values.

mal fluctuations throughout the episode. Consequently, the average speed computed over time closely reflects the instantaneous speed, and the resulting travel time and energy consumption align well with the analytical cost model.

Under medium and high traffic densities, the relationship between average speed and cost deviates increasingly from the analytical curves. In these settings, the reported average speed represents a temporal mean over highly variable speed profiles that include frequent acceleration, deceleration, and lane change maneuvers induced by interactions with surrounding vehicles. While different policies may exhibit similar average speeds, their underlying speed trajectories can differ substantially, leading to different travel times and energy expenditures. Therefore, when surrounding vehicles are added, these variations become more pronounced, resulting in small deviations between the analytically predicted costs and the observed costs from the experiments. Nonetheless, when costs are normalized per meter, the best policy in terms of total cost achieves TCOP per meter close to the analytical prediction: exactly 0.0012 euros/m for zero traffic and 0.0013 euros/m for medium and high traffic. Detailed numerical results for all traffic conditions and policies are provided in Appendix E.

Moreover, as traffic density increases, there is a scarcity of policies whose average speed approaches the analytical optimum. Higher traffic density constrains the ego vehicle's

ability to accelerate and sustain high cruising speeds, limiting its ability to operate near the analytically optimal speed. The combined effect of speed variability and repeated transient maneuvers explains the progressively larger divergence from analytical cost values observed at higher traffic densities. These results highlight that interactive traffic fundamentally alters the steady-state speed–cost relationship, and demonstrate that the proposed MORL framework adapts by learning policies that optimize cumulative performance over entire driving trajectories while balancing operational costs and feasibility under realistic traffic constraints.

5   Conclusion

We developed a multi-objective reinforcement learning framework for autonomous truck tactical decision making by introducing a multi-objective Proximal Policy Optimization (MOPPO) architecture combined with Generalized Policy Improvement with Linear Support (GPI-LS). Experiments conducted in a realistic highway driving simulator show that the proposed approach efficiently approximates the Pareto frontier and enables flexible control over safety, time, and energy trade-offs. These results demonstrate the effectiveness of the method for heavy-duty vehicle applications and open up new possibilities for deploying adaptive, preference-aware autonomous driving policies in real-world logistics operations.

References

[Abdallaoui *et al.*, 2023] Sara Abdallaoui, Halima Ikaouassen, Ali Kribèche, Ahmed Chaibet, and El-Hassane Aglzim. Advancing autonomous vehicle control systems: An in-depth overview of decision-making and manoeuvre execution state of the art. *The Journal of Engineering*, 2023(11):e12333, 2023.

[Abouelazm *et al.*, 2024] Ahmed Abouelazm, Jonas Michel, and J. Marius Zöllner. A review of reward functions for reinforcement learning in the context of autonomous driving. In *2024 IEEE Intelligent Vehicles Symposium (IV)*, pages 156–163, 2024.

[Alegre *et al.*, 2023] Lucas N. Alegre, Ana L. C. Bazzan, Diederik M. Roijers, Ann Nowé, and Bruno C. da Silva. Sample-efficient multi-objective learning via generalized policy improvement prioritization. In *Proceedings of the 2023 International Conference on Autonomous Agents and Multiagent Systems*, AAMAS '23, page 2003–2012, Richland, SC, 2023. International Foundation for Autonomous Agents and Multiagent Systems.

[Barreto *et al.*, 2017] André Barreto, Will Dabney, Rémi Munos, Jonathan J. Hunt, Tom Schaul, Hado van Hasselt, and David Silver. Successor features for transfer in reinforcement learning. In *Proceedings of the 31st International Conference on Neural Information Processing Systems*, NIPS'17, page 4058–4068, Red Hook, NY, USA, 2017. Curran Associates Inc.

[Brewitt *et al.*, 2021] Cillian Brewitt, Balint Gyevnar, Samuel Garcin, and Stefano V Albrecht. Grit: Fast, interpretable, and verifiable goal recognition with learned decision trees for autonomous driving. In *2021 IEEE/RSJ International Conference on Intelligent Robots and Systems (IROS)*, pages 1023–1030. IEEE, 2021.

[Cai *et al.*, 2023] Xin-Qiang Cai, Pushi Zhang, Li Zhao, Jiang Bian, Masashi Sugiyama, and Ashley Llorens. Distributional pareto-optimal multi-objective reinforcement learning. In A. Oh, T. Naumann, A. Globerson, K. Saenko, M. Hardt, and S. Levine, editors, *Advances in Neural Information Processing Systems*, volume 36, pages 15593–15613. Curran Associates, Inc., 2023.

[Campbell *et al.*, 2010] Mark Campbell, Magnus Egerstedt, Jonathan P How, and Richard M Murray. Autonomous driving in urban environments: approaches, lessons and challenges. *Philosophical Transactions of the Royal Society A: Mathematical, Physical and Engineering Sciences*, 368(1928):4649–4672, 2010.

[Eleonora *et al.*, 2023] Andreotti Eleonora, Boyraz Pinar, et al. Potential impact of autonomous vehicles in mixed traffic from simulation using real traffic flow. *Journal of Intelligent and Connected Vehicles*, 6(1):1–15, 2023.

[Engström *et al.*, 2018] Johan Engström, Richard Bishop, Steven E Shladover, Michael C Murphy, Laurence O'Rourke, Tom Voege, Bob Denaro, Richard Demato, and Divya Demato. Deployment of automated trucking: challenges and opportunities. *Road Vehicle Automation 5*, pages 149–162, 2018.

[Erdmann, 2014] Jakob Erdmann. Lane-changing model in sumo. In *Proceedings of the SUMO2014 Modeling Mobility with Open Data*, volume 24 of *Reports of the DLR-Institute of Transportation SystemsProceedings*, 2014.

[Felten *et al.*, 2023] Florian Felten, Lucas N. Alegre, Ann Nowé, Ana L. C. Bazzan, El-Ghazali Talbi, Grégoire Danoy, and Bruno C. da Silva. A toolkit for reliable benchmarking and research in multi-objective reinforcement learning. In *Proceedings of the 37th International Conference on Neural Information Processing Systems*, NIPS '23, Red Hook, NY, USA, 2023. Curran Associates Inc.

[Hayes *et al.*, 2022] Conor F. Hayes, Roxana Rădulescu, Eugenio Bargiacchi, Johan Källström, Matthew Macfarlane, Mathieu Reymond, Timothy Verstraeten, Luisa M. Zintgraf, Richard Dazeley, Fredrik Heintz, Enda Howley, Athirai A. Irissappane, Patrick Mannion, Ann Nowé, Gabriel Ramos, Marcello Restelli, Peter Vamplew, and Diederik M. Roijers. A practical guide to multi-objective reinforcement learning and planning. *Autonomous Agents and Multi-Agent Systems*, 36(1), April 2022.

[He and Lv, 2023] Xiangkun He and Chen Lv. Towards energy-efficient autonomous driving: A multi-objective reinforcement learning approach. *IEEE/CAA Journal of Automatica Sinica*, 10(5):1329–1331, 2023.

[Hoel *et al.*, 2020] Carl-Johan Hoel, Krister Wolff, and Leo Laine. Tactical decision-making in autonomous driving by reinforcement learning with uncertainty estimation. In *2020 IEEE Intelligent Vehicles Symposium (IV)*, pages 1563–1569, 2020.

[Isaksson Palmqvist, 2016] Mia Isaksson Palmqvist. Model predictive control for autonomous driving of a truck, 2016.

[Kiran *et al.*, 2022] B Ravi Kiran, Ibrahim Sobh, Victor Talpaert, Patrick Mannion, Ahmad A. Al Sallab, Senthil Yogamani, and Patrick Pérez. Deep reinforcement learning for autonomous driving: A survey. *IEEE Transactions on Intelligent Transportation Systems*, 23(6):4909–4926, 2022.

[Knox *et al.*, 2023] W. Bradley Knox, Alessandro Allievi, Holger Banzhaf, Felix Schmitt, and Peter Stone. Reward (mis)design for autonomous driving. *Artificial Intelligence*, 316:103829, 2023.

[Krauss *et al.*, 1997] S. Krauss, P. Wagner, and C. Gawron. Metastable states in a microscopic model of traffic flow. *Phys. Rev. E*, 55, 1997.

[Musa *et al.*, 2021] Alessia Musa, Michele Pipicelli, Matteo Spano, Francesco Tufano, Francesco De Nola, Gabriele Di Blasio, Alfredo Gimelli, Daniela Anna Misul, and Gianluca Toscano. A review of model predictive controls applied to advanced driver-assistance systems. *Energies*, 14(23), 2021.

[Nilsson *et al.*, 2015] Peter Nilsson, Leo Laine, Niels van Duijkeren, and Bengt Jacobson. Automated highway lane changes of long vehicle combinations: A specific comparison between driver model based control and non-linear

model predictive control. In *2015 International Symposium on Innovations in Intelligent SysTems and Applications (INISTA)*, pages 1–8, 2015.

[Paden *et al.*, 2016] Brian Paden, Michal Čáp, Sze Zheng Yong, Dmitry Yershov, and Emilio Frazzoli. A survey of motion planning and control techniques for self-driving urban vehicles. *IEEE Transactions on intelligent vehicles*, 1(1):33–55, 2016.

[Pathare *et al.*, 2023] Deepthi Pathare, Leo Laine, and Morteza Haghir Chehreghani. Improved tactical decision making and control architecture for autonomous truck in sumo using reinforcement learning. In *2023 IEEE International Conference on Big Data (BigData)*, pages 5321–5329, 2023.

[Pathare *et al.*, 2026] Deepthi Pathare, Leo Laine, and Morteza Haghir Chehreghani. Tactical decision making for autonomous trucks by deep reinforcement learning with total cost of operation based reward. *Artificial Intelligence Review*, 59(1):27, 2026.

[Schulman *et al.*, 2015] John Schulman, Philipp Moritz, Sergey Levine, Michael Jordan, and Pieter Abbeel. High-dimensional continuous control using generalized advantage estimation, 2015.

[Schulman *et al.*, 2017] John Schulman, Filip Wolski, Prafulla Dhariwal, Alec Radford, and Oleg Klimov. Proximal policy optimization algorithms, 2017.

[Schwarting *et al.*, 2018] Wilko Schwarting, Javier Alonso-Mora, and Daniela Rus. Planning and decision-making for autonomous vehicles. *Annual Review of Control, Robotics, and Autonomous Systems*, 1(1):187–210, 2018.

[Surmann *et al.*, 2025] Hendrik Surmann, Jorge de Heuvel, and Maren Bennewitz. Multi-objective reinforcement learning for adaptive personalized autonomous driving. *arXiv preprint arXiv:2505.05223*, 2025.

[Treiber *et al.*, 2000] Martin Treiber, Ansgar Hennecke, and Dirk Helbing. Congested traffic states in empirical observations and microscopic simulations. *Physical review E*, 62(2):1805, 2000.

[Xu *et al.*, 2018] Xin Xu, Lei Zuo, Xin Li, Lilin Qian, Junkai Ren, and Zhenping Sun. A reinforcement learning approach to autonomous decision making of intelligent vehicles on highways. *IEEE Transactions on Systems, Man, and Cybernetics: Systems*, 50(10):3884–3897, 2018.

[Xu *et al.*, 2020] Jie Xu, Yunsheng Tian, Pingchuan Ma, Daniela Rus, Shinjiro Sueda, and Wojciech Matusik. Prediction-guided multi-objective reinforcement learning for continuous robot control. In Hal Daumé III and Aarti Singh, editors, *Proceedings of the 37th International Conference on Machine Learning*, volume 119 of *Proceedings of Machine Learning Research*, pages 10607–10616. PMLR, 13–18 Jul 2020.

[Zhang *et al.*, 2020] Jian Zhang, Kunrun Wu, Min Cheng, Min Yang, Yang Cheng, and Shen Li. Safety evaluation for connected and autonomous vehicles' exclusive lanes considering penetrate ratios and impact of trucks using surrogate safety measures. *Journal of advanced transportation*, 2020(1):5847814, 2020.

[Zhang *et al.*, 2023] Linzi Zhang, Zhiquan Qi, and Yong Shi. Multi-objective reinforcement learning – concept, approaches and applications. *Procedia Computer Science*, 221:526–532, 2023. Tenth International Conference on Information Technology and Quantitative Management (ITQM 2023).

[Zhou *et al.*, 2023] Zixian Zhou, Mengda Huang, Feiyang Pan, Jia He, Xiang Ao, Dandan Tu, and Qing He. Gradient-adaptive pareto optimization for constrained reinforcement learning. *Proceedings of the AAAI Conference on Artificial Intelligence*, 37(9):11443–11451, Jun. 2023.

A Multi-Objective Reinforcement Learning Literature

Recent surveys emphasize the need for specialized MORL methods beyond naive weighting objectives [Hayes *et al.*, 2022; Zhang *et al.*, 2023]. The paper [Hayes *et al.*, 2022] notes that if the user's utility function is known and static, a single-policy approach (learning one policy conditioned on preferences) may suffice, whereas if the utility is unknown or may change, one should compute a *coverage set* of Pareto-optimal policies (a multi-policy solution). Single-policy methods (e.g., universal value function approximators or multi-head networks) aim to generalize across preferences, while multi-policy approaches explicitly approximate the Pareto front. These approaches also differ in whether they are model-free or model-based, on-policy or off-policy, and in how they reuse past experience. In short, MORL methods can be classified by solution concept (single vs. multi policy), optimization strategy, and how they trade off exploration versus reuse of data.

Many recent works instantiate these categories with concrete algorithms. The paper [Xu *et al.*, 2020] proposes a prediction-guided evolutionary MORL algorithm for continuous control that extends deep RL with an analytic improvement model using evolutionary algorithm. At each generation, they fit a model of expected performance improvement and solve a guiding optimization to select which preference vectors to train next. Another work [Zhou *et al.*, 2023] focuses on constrained RL and proposes Gradient-Adaptive Constrained Policy Optimization (GCPO), which rebalances policy gradients adaptively to emphasize under-optimized objectives while enforcing cost constraints. The paper [Cai *et al.*, 2023] extends Pareto-optimality to full return distributions, introducing Distributional Pareto-Optimal MORL (DPMORL), which captures uncertainty in returns—an important consideration in safety-critical domains such as autonomous driving. Meanwhile, another work [Felten *et al.*, 2023] releases *MO-Gymnasium* and *MORL-Baselines*, providing standardized environments and algorithmic implementations that enable rigorous benchmarking of MORL methods.

B Traffic Modeling

We created a custom RL environment for autonomous trucks in highway traffic as illustrated in Figure 4. The surrounding vehicles are modeled using the Krauss car following model [Krauss *et al.*, 1997] and LC2013 lane change model [Erdmann, 2014] in SUMO. Each surrounding vehicle is assigned a maximum speed sampled from a empirically motivated distribution. The traffic parameters used in this study are provided in Table 1.

C Detailed Architecture

The decision making and control architecture is hierarchical integrating RL with low-level controllers as depicted in Figure 5. It is adapted from the paper [Pathare *et al.*, 2026], extended for MORL.

We separate the high level and low level decision making between MORL agent and low-level controllers. The agent

Table 1: Traffic simulation parameters.

Parameter	Value
Length of highway segment (l_{road})	3000 m
Moving window size (l_{window})	400 m
Heterogeneous vehicle ratio (trucks)	0.2
Heterogeneous vehicle ratio (cars)	0.8
Car speed distribution	$\mathcal{N}(23, 3.8)$ m/s
Truck speed distribution	$\mathcal{N}(20, 0.8)$ m/s
Maximum speed of ego truck	25 m/s
Maximum acceleration of ego truck	$0.1 \ m/s^2$
Maximum deceleration of ego truck	$6 \ m/s^2$
Maximum episode length	200

has a discrete action space which includes high level decisions about longitudinal and lateral controls. The longitudinal actions include changing the desired speed or desired timegap with the vehicle. Lateral actions include changing the lane to left or right. The actions space is given below.

1. Set short time gap with leading vehicle (1s)

2. Set medium time gap with leading vehicle (2s)

3. Set long time gap with leading vehicle (3s)

4. Increase the desired speed by 1 m/s

5. Decrease the desired speed by 1 m/s

6. Maintain current desired speed and time gap

7. Change lane to left

8. Change lane to right

When one of the longitudinal action is chosen it triggers the longitudinal controller which compute the acceleration/deceleration using the set desired speed and timegap. We use Intelligent Driver Model (IDM) [Treiber *et al.*, 2000] given by,

$$\dot{v}_\alpha = \frac{\mathrm{d}v_\alpha}{\mathrm{d}t} = a\left(1 - \left(\frac{v_\alpha}{v_0}\right)^\delta - \left(\frac{s^*(v_\alpha, \Delta v_\alpha)}{s_\alpha}\right)^2\right),$$

$$s^*(v_\alpha, \Delta v_\alpha) = s_0 + v_\alpha T + \frac{v_\alpha \Delta v_\alpha}{2\sqrt{ab}}$$

(11)

where α is the ego vehicle and $\alpha - 1$ is the leading vehicle. v denotes the velocity and l denotes the length of the vehicle. $s_\alpha := x_{\alpha-1} - x_\alpha - l_{\alpha-1}$ is the net distance and $\Delta v_\alpha := v_\alpha - v_{\alpha-1}$ is the velocity difference. v_0 (desired velocity), s_0 (minimum spacing), T (desired time gap), a (maximum acceleration), and b (comfortable braking deceleration) are model parameters.

A new acceleration is computed for the truck and the resulting speed is set to the vehicle every 0.1s. This process continues for a total duration of 1s, after which the RL agent chooses the next high level action. If a lateral action is chosen by the agent, the lateral controller initiates the lane change. Lane change is performed using the default LC2013 lane change model [Erdmann, 2014] in SUMO. The lane width is set to $3.2m$ and the lateral speed of the truck is set to $0.8m/s$.
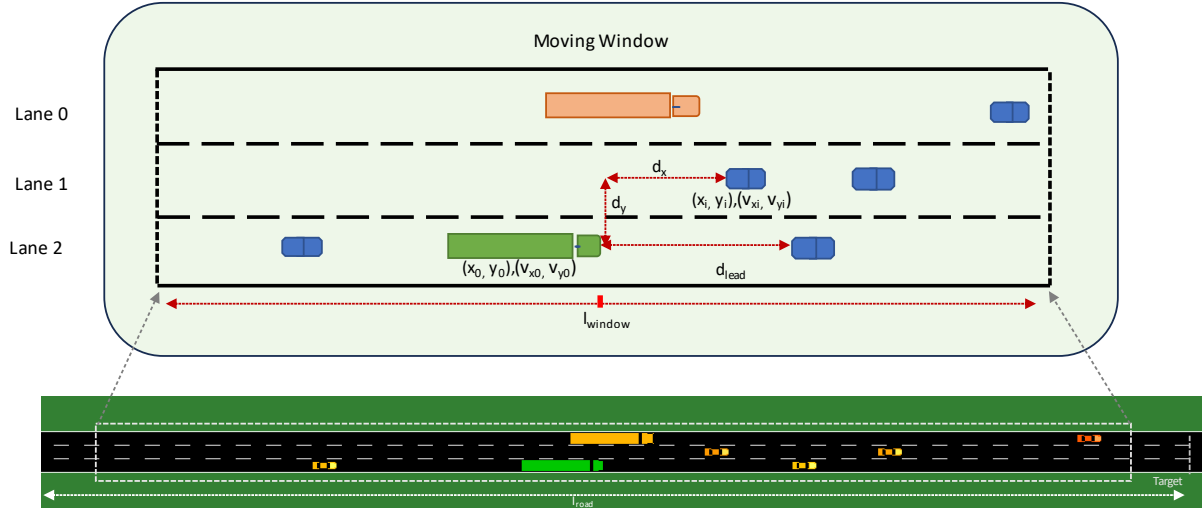
Figure 4: Simulated traffic environment in SUMO with the illustration of moving window.
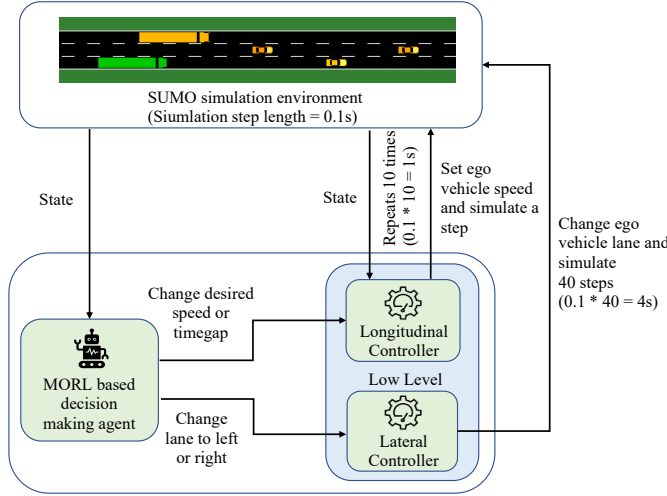

Figure 5: Overview of the architecture adapted from [Pathare *et al.*, 2026], extended for multi-objective learning

Hence, in total, it takes $4s$ to complete a lane change, following which RL chooses the next high level action.

The state space of RL includes the observations for ego truck and surrounding vehicles. Following are the observations for the ego vehicle:

1. Longitudinal position

2. Longitudinal speed

3. Lane change state

4. State of left indicator

5. State of right indicator

6. Lane number

7. Length of the vehicle

8. Width of the vehicle

9. Target (leading) vehicle distance

Following are the observations for each vehicle in the sensor range of the ego vehicle:

1. Relative longitudinal distance from ego vehicle

2. Relative lateral distance from ego vehicle

3. Relative longitudinal speed with ego vehicle

4. Lane change state

5. Lane number

6. State of left indicator

7. State of right indicator

8. Length of the vehicle

9. Width of the vehicle

D Reward Computation

As mentioned in Section 2.3, the reward vector consists of the following components.

$$r_t = [I_{tar}R_{tar} - I_c P_c, -C_{dr}\Delta t, -C_{el}e_t]^T \quad (12)$$

C_{el} is the electricity cost, e_t is the electricity consumed at time step t, C_{dr} is the driver cost and Δt is the duration of a time step. Δt would be $1s$ for a longitudinal action and $4s$ for a lateral action. The electricity consumed during the time step t (e_t) is calculated as,

$$e_t = f_t\, v_t\, \Delta t, \quad (13)$$

where f_t, force at time step t is given by,

$$f_t = m\, a_t + \frac{1}{2}C_d\, A_f\, \rho_{\text{air}}\, v^2 + m\, g\, C_r$$
$$+ m\, g\, \sin(\arctan(\frac{\text{slope}}{100})) \quad (14)$$

Here m is the mass of the vehicle, C_d is the coefficient of air drag, A_f is the frontal area, ρ_{air} is the air density, C_r is the

coefficient of rolling resistance, g is the acceleration due to gravity and a is the acceleration of the vehicle at time step t. We use a road segment with 0 slope in this study. The parameter values are given in Table 2.

Table 2: Parameter values used for reward computation.

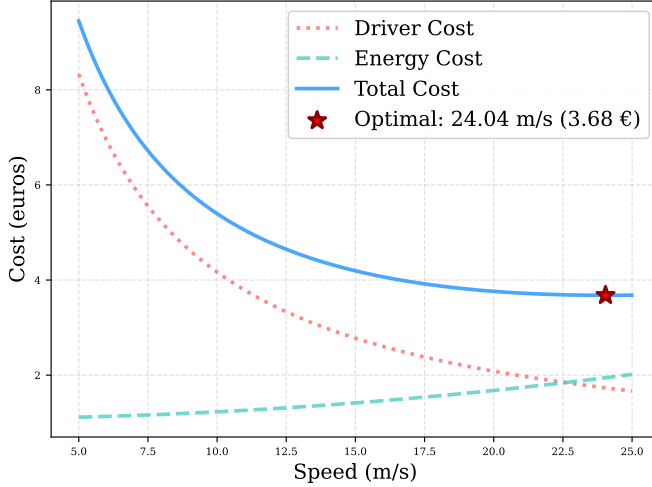| Parameter	Value
R_{tar}	4.41
P_c	1000
C_{el}	0.5 euro per kwh
C_{dr}	50 euro per hour
m	44000 kg
C_d	0.6
A_f	$10 \; m^2$
ρ_{air}	$1.2 \; kg/m^3$
g	$9.81 \; m/s^2$
C_r	0.006

E Detailed Results

Figure 6: Analytical predictions for optimal speed and cost in zero traffic situation.

Here, we present detailed results for the trained models across different traffic settings. For each setting, the framework was trained for 100 iterations (i.e., $N = 100$ in Algorithm 1), with each iteration consisting of 10,000 training steps (i.e., $N_S = 10,000$ in Algorithm 2), using a learning rate of 3×10^{-4}. The analytical predictions under the zero-traffic assumption are provided in Figure 6. Figures 7, 8, and 9 illustrate the Pareto fronts shown in Figure 2, where each policy is labeled by its corresponding number. A detailed quantitative evaluation of each policy, averaged over 5 episodes, is given in Tables 3, 4, and 5.

The success rate indicates the number of episodes that reached the target within the maximum allowed steps, while the failure rate indicates episodes terminated due to collisions. Notably, the failure rate is zero for all policies under all

traffic conditions considered. The max step rate corresponds to episodes that terminated after reaching the maximum number of steps without completing the target. The target distance is approximately 3000 m, with minor variations depending on the truck's start and end positions.

The results are easily interpretable. For policies that tries to minimize energy cost have low average speed and therefore higher time to reach target and consequently higher driver cost. For policies that tries to minimize driver cost have higher average speed and consequently higher energy cost. In the zero-traffic case, for successful policies, the best TCOP achieved is around 3.75 euros for 3 km, which is comparable to the analytical cost of 3.68 euros. The best TCOP per meter is 0.0012 euros/m in zero traffic case which is same as the corresponding analytical value. In medium and high traffic, policies span a wider range of average speeds, which directly affects energy cost and driver cost. The best total cost achieved is 0.0013 euros/m in both medium and high traffic, indicating that even under denser traffic conditions, the policies maintain operational efficiency comparable to that of the analytical values (0.0012 euros/m).

We also observed that our GPI-LS framework, which uses a policy-based approach (MOPPO), is computationally more efficient than the value-based GPI-LS [Alegre *et al.*, 2023] as implemented in [Felten *et al.*, 2023]. In our RL environment for truck driving, training the latter for 7.5×10^5 steps required approximately 35 hours, whereas the same training using our framework completed in roughly 30 hours. Experiments were conducted on a Linux cluster with two AMD EPYC 7763 64-core processors.
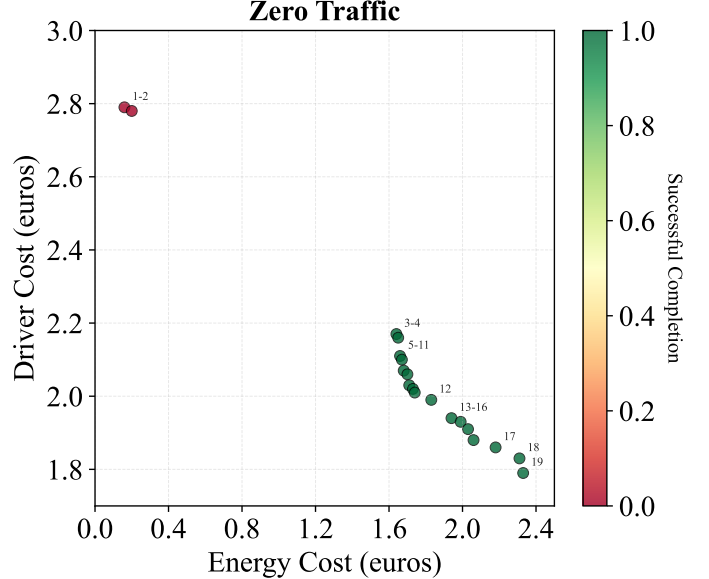

Figure 7: Pareto Front showing the trade off between driver cost and energy cost in zero traffic, along with the success rate. The annotated numbers denote the policy numbers referred in the Table 3

Table 3: Evaluation of Pareto-optimal policies in Zero Traffic

Policy Number	Success Rate (%)	Failure Rate (%)	Max Step Rate (%)	Avg. Speed (m/s)	Energy Cost (euros)	Driver Cost (euros)	Distance (m)	TCOP (euros)	TCOP per m (euros)
1	0.0	0.0	100.0	1.6	0.16	2.79	338	2.95	0.0087
2	0.0	0.0	100.0	1.8	0.20	2.78	374	2.98	0.0080
3	100.0	0.0	0.0	19.3	1.64	2.17	3006	3.81	0.0013
4	100.0	0.0	0.0	19.4	1.65	2.16	3006	3.81	0.0013
5	100.0	0.0	0.0	19.7	1.66	2.11	2996	3.77	0.0013
6	100.0	0.0	0.0	19.8	1.67	2.10	2992	3.77	0.0013
7	100.0	0.0	0.0	20.1	1.68	2.07	2985	3.75	0.0013
8	100.0	0.0	0.0	20.3	1.70	2.06	2997	3.76	0.0013
9	100.0	0.0	0.0	20.5	1.71	2.03	2998	3.74	0.0012
10	100.0	0.0	0.0	20.7	1.73	2.02	3013	3.75	0.0012
11	100.0	0.0	0.0	20.8	1.74	2.01	3009	3.75	0.0012
12	100.0	0.0	0.0	21.1	1.83	1.99	3019	3.82	0.0013
13	100.0	0.0	0.0	21.5	1.94	1.94	3020	3.88	0.0013
14	100.0	0.0	0.0	21.6	1.99	1.93	3022	3.92	0.0013
15	100.0	0.0	0.0	21.8	2.03	1.91	3004	3.94	0.0013
16	100.0	0.0	0.0	21.8	2.06	1.88	2999	3.94	0.0013
17	100.0	0.0	0.0	22.4	2.18	1.86	3036	4.04	0.0013
18	100.0	0.0	0.0	22.6	2.31	1.83	2987	4.14	0.0014
19	100.0	0.0	0.0	23.2	2.33	1.79	2987	4.12	0.0014

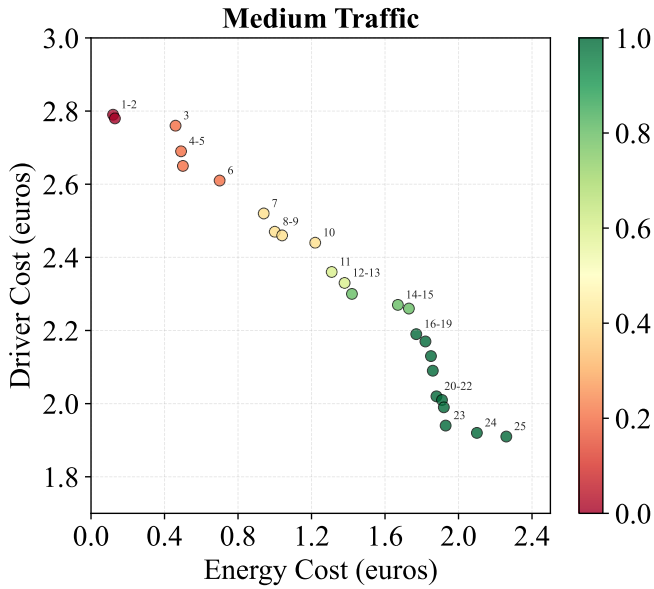Figure 8: Pareto Front showing the trade off between driver cost and energy cost in medium traffic, along with the success rate. The annotated numbers denote the policy numbers referred in the Table 4
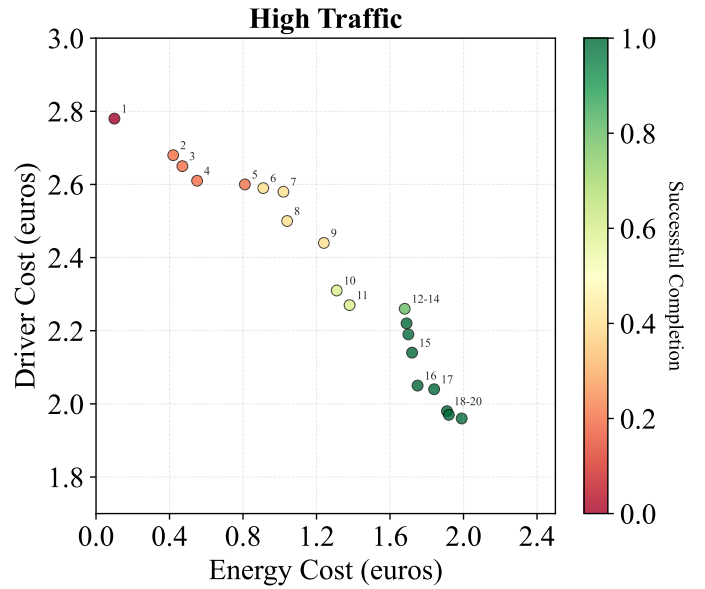
Figure 9: Pareto Front showing the trade off between driver cost and energy cost in high traffic, along with the success rate. The annotated numbers denote the policy numbers referred in the Table 5

Table 4: Evaluation of Pareto-optimal policies in Medium Traffic

Policy Number	Success Rate (%)	Failure Rate (%)	Max Step Rate (%)	Avg. Speed (m/s)	Energy Cost (euros)	Driver Cost (euros)	Distance (m)	TCOP (euros)	TCOP per m (euros)
1	0.0	0.0	100.0	1.4	0.12	2.79	210	2.91	0.0138
2	0.0	0.0	100.0	1.5	0.13	2.78	406	2.91	0.0072
3	20.0	0.0	80.0	4.9	0.46	2.76	901	3.22	0.0036
4	20.0	0.0	80.0	5.2	0.49	2.69	882	3.18	0.0036
5	20.0	0.0	80.0	5.4	0.50	2.65	952	3.15	0.0033
6	20.0	0.0	80.0	7.5	0.70	2.61	1275	3.31	0.0026
7	40.0	0.0	60.0	9.3	0.94	2.52	1533	3.46	0.0023
8	40.0	0.0	60.0	10.0	1.00	2.47	1515	3.47	0.0023
9	40.0	0.0	60.0	10.5	1.04	2.46	1798	3.50	0.0019
10	40.0	0.0	60.0	11.6	1.22	2.44	1826	3.66	0.0020
11	60.0	0.0	40.0	14.0	1.31	2.36	2326	3.67	0.0016
12	60.0	0.0	40.0	14.4	1.38	2.33	2307	3.71	0.0016
13	80.0	0.0	20.0	15.7	1.42	2.30	2400	3.72	0.0015
14	80.0	0.0	20.0	17.0	1.67	2.27	2751	3.94	0.0014
15	80.0	0.0	20.0	17.6	1.73	2.26	2654	3.99	0.0015
16	100.0	0.0	0.0	18.6	1.77	2.19	3040	3.96	0.0013
17	100.0	0.0	0.0	19.2	1.82	2.17	2976	3.99	0.0013
18	100.0	0.0	0.0	19.6	1.85	2.13	3005	3.98	0.0013
19	100.0	0.0	0.0	19.5	1.86	2.09	3025	3.95	0.0013
20	100.0	0.0	0.0	20.4	1.88	2.02	3086	3.90	0.0013
21	100.0	0.0	0.0	20.3	1.91	2.01	3028	3.92	0.0013
22	100.0	0.0	0.0	20.6	1.92	1.99	3124	3.91	0.0013
23	100.0	0.0	0.0	21.2	1.93	1.94	2989	3.87	0.0013
24	100.0	0.0	0.0	21.1	2.10	1.92	3011	4.02	0.0013
25	100.0	0.0	0.0	21.3	2.26	1.91	3137	4.17	0.0013

Table 5: Evaluation of Pareto-optimal policies in High Traffic

Policy Number	Success Rate (%)	Failure Rate (%)	Max Step Rate (%)	Avg. Speed (m/s)	Energy Cost (euros)	Driver Cost (euros)	Distance (m)	TCOP (euros)	TCOP per m (euros)
1	0.0	0.0	100.0	1.3	0.10	2.78	341	2.88	0.0084
2	20.0	0.0	80.0	4.9	0.42	2.68	904	3.10	0.0034
3	20.0	0.0	80.0	5.1	0.47	2.65	798	3.12	0.0039
4	20.0	0.0	80.0	5.9	0.55	2.61	885	3.16	0.0036
5	20.0	0.0	80.0	7.9	0.81	2.60	1444	3.41	0.0024
6	40.0	0.0	60.0	9.5	0.91	2.59	1786	3.50	0.0020
7	40.0	0.0	60.0	9.1	1.02	2.58	1492	3.60	0.0024
8	40.0	0.0	60.0	10.7	1.04	2.50	1687	3.54	0.0021
9	40.0	0.0	60.0	12.1	1.24	2.44	2052	3.68	0.0018
10	60.0	0.0	40.0	13.5	1.31	2.31	2155	3.62	0.0017
11	60.0	0.0	40.0	14.1	1.38	2.27	2087	3.65	0.0017
12	80.0	0.0	20.0	17.6	1.68	2.26	2714	3.94	0.0015
13	100.0	0.0	0.0	18.3	1.69	2.22	2955	3.91	0.0013
14	100.0	0.0	0.0	18.4	1.70	2.19	3031	3.89	0.0013
15	100.0	0.0	0.0	18.7	1.72	2.14	2912	3.86	0.0013
16	100.0	0.0	0.0	19.5	1.75	2.05	2987	3.80	0.0013
17	100.0	0.0	0.0	19.6	1.84	2.04	2794	3.88	0.0014
18	100.0	0.0	0.0	20.3	1.91	1.98	2941	3.89	0.0013
19	100.0	0.0	0.0	20.3	1.92	1.97	3069	3.89	0.0013
20	100.0	0.0	0.0	20.4	1.99	1.96	3035	3.95	0.0013